Polymer Self-Consistent Field Theory in Bulk and under Confinement

Yi-Xin Liu
lyx@fudan.edu.cn

Department of Marcomolecular Science
Fudan University
Shanghai, China

March 10, 2014

@ASML Brion, Santa Clara, CA

Outline

- Introduction to the self-consistent field theory (SCFT)
  - Fundamentals
  - Applications
- Implementation of SCFT — the `Polyorder` project
- My research works on SCFT
  - Self-assembly of weakly charged block copolymers
  - Self-assembly of block copolymers confined by interacting walls
  - Thermodynamics of polymer brushes on interacting substrates
- Summary
- Acknowledgments

Introduction to the Self-Consistent Field Theory

- Fundamentals
- Applications

Fundamentals of SCFT

Particle-Based and Field-Based Methods

Method	SCFT	SCMF	TICG
Schematics	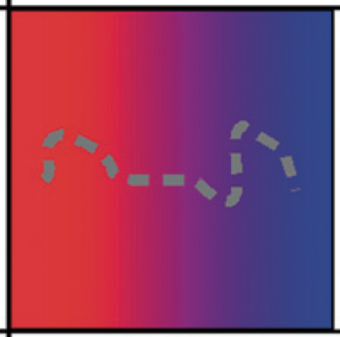	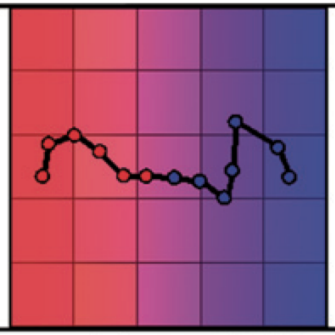	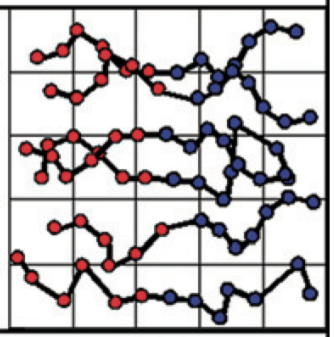
Degrees of freedom	fields	particles and fields	particles
Implementation	numerical resolution	two-step cycle	genuine MC simulation
Fluctuations	no	yes	
Free energy	known	requires additional work	
System dimensionality	often 2D	3D	

Fig. 1 Comparison between three methods applicable to the standard model of block copolymers: self-consistent field theory (SCFT), single-chain in mean field (SCMF) simulations and theoretically informed coarse grain (TICG) simulations. In SCFT, chains are described implicitly by a diffusion process in a field, which represents the average effect of the local environment. In SCMF simulations, each chain is described explicitly and evolves in a field which fluctuates, since it is periodically recomputed from the chain configurations. No fields are introduced in the TICG simulations, and chains interact directly with one another.

Detcheverry, F. A.; et al. *Soft Matter* **2009**, *5*, 4858.

Fundamentals of SCFT

Key Concept of SCFT

Polymer Chains experience a potential field that is generated by other chains.

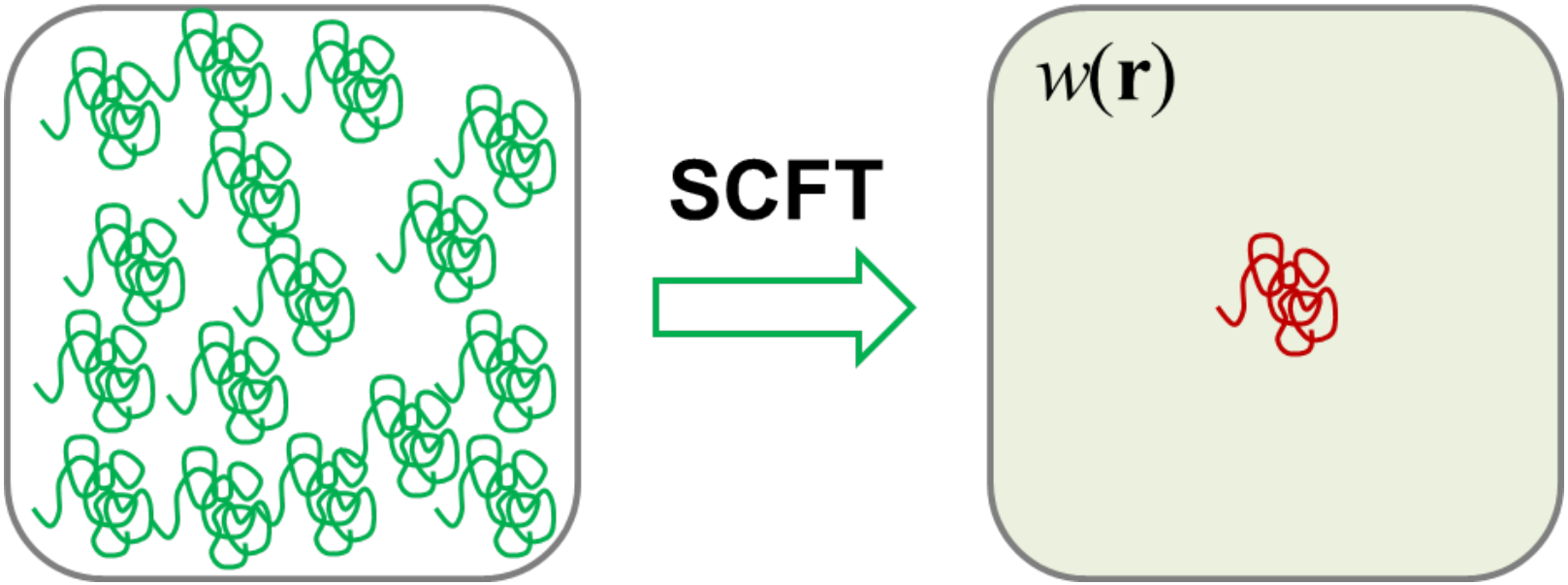

Below, we describe SCFT for melt of n identical AB diblock copolymer chains, each with N segments of which a fraction f forms the A block.

Fredrickson, G. H. *The Equilibrium Theory of Inhomogeneous Polymers* **2006**, Clarendon Press: Oxford.

Fundamentals of SCFT

Segment Density Distributions

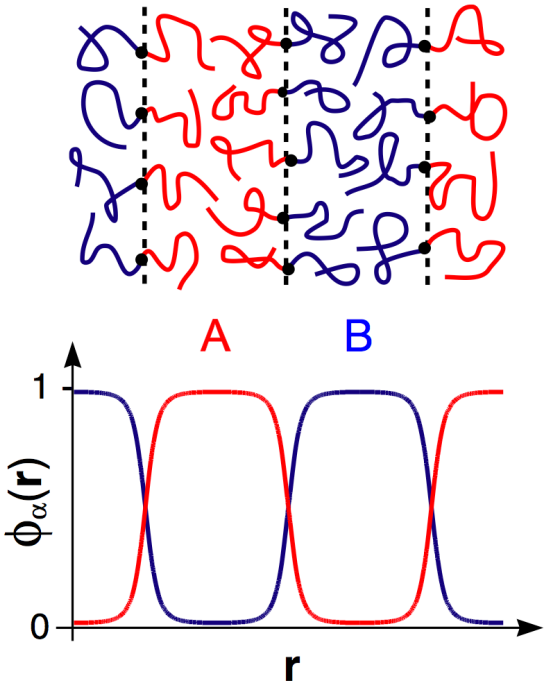

Figure 3. Schematic diagram showing the molecular self-assembly within the lamellar (L) phase with the corresponding ensemble-averaged segment distributions, $\phi_A(\boldsymbol{r})$ and $\phi_B(\boldsymbol{r})$.

Matsen, M. W. *J. Phys. Cond. Matter* **2002**, *14*, 21.

$$\hat{\phi}_A(\mathbf{r}) = \frac{N}{\rho_0} \sum_{\alpha=1}^{n} \int_0^f \delta(\mathbf{r} - \mathbf{R}_\alpha(s)) ds$$

$$\hat{\phi}_B(\mathbf{r}) = \frac{N}{\rho_0} \sum_{\alpha=1}^{n} \int_f^1 \delta(\mathbf{r} - \mathbf{R}_\alpha(s)) ds$$

Their ensemble averages are

$$\phi_A(\mathbf{r}) \equiv \langle \hat{\phi}_A(\mathbf{r}) \rangle$$

$$\phi_B(\mathbf{r}) \equiv \langle \hat{\phi}_B(\mathbf{r}) \rangle$$

Fundamentals of SCFT

Coarse Grained Gaussian Model

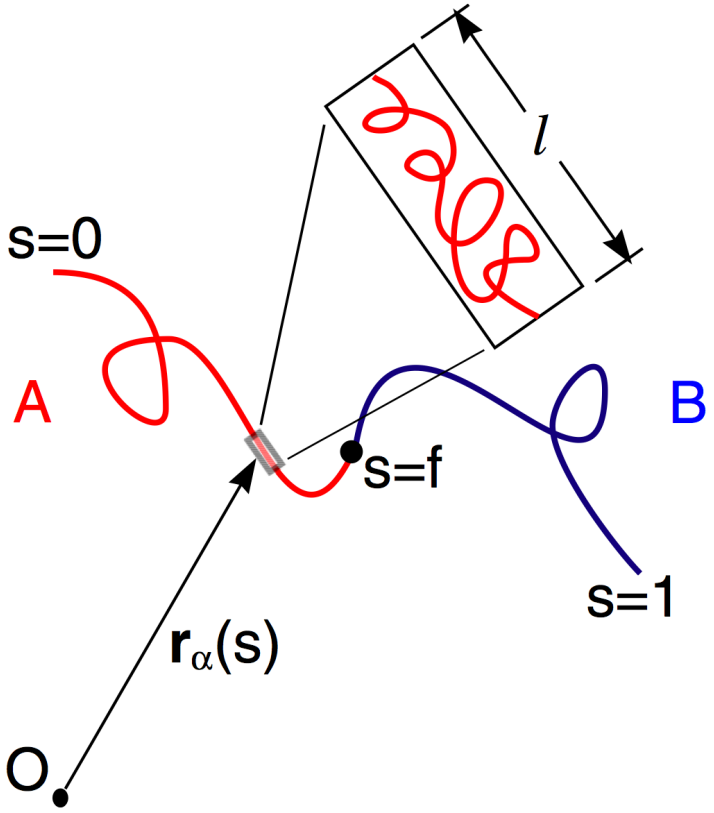

$$\beta U_0\left[\mathbf{R}_\alpha(s)\right] = \sum_\alpha \int_0^1 \frac{3}{2a^2 N}\left|\frac{\partial \mathbf{R}_\alpha(s)}{\partial s}\right|^2 ds$$

Matsen, M. W. *J. Phys. Cond. Matter* **2002**, *14*, 21.

Fundamentals of SCFT

Segment Interactions

$$\beta U_1 \left[\mathbf{R}_\alpha(s)\right] = \chi\rho_0 \int \hat{\phi}_A(\mathbf{r})\hat{\phi}_B(\mathbf{r})d\mathbf{r}$$

Fredrickson, G. H. *The Equilibrium Theory of Inhomogeneous Polymers* **2006**, Clarendon Press: Oxford.

Fundamentals of SCFT

Partition Function

$$Z = \frac{1}{n!\lambda_T^{nN}} \int d\mathbf{r}^{nN} \exp\left(-\beta U_0\left[\mathbf{R}_\alpha(s)\right] - \beta U_1\left[\mathbf{R}_\alpha(s)\right]\right) \delta(\hat{\phi}_A(\mathbf{r}) + \hat{\phi}_B(\mathbf{r}) - 1)$$

Fredrickson, G. H. *The Equilibrium Theory of Inhomogeneous Polymers* **2006**, Clarendon Press: Oxford.

Fundamentals of SCFT

From Particle to Field: The Hubbard-Stratonovich Transformation

$$Z = Z_0 \int \mathcal{D}\phi_A \mathcal{D}\phi_B \mathcal{D}w_A \mathcal{D}w_B \mathcal{D}\eta \exp(-H)$$

with

$$H = \int d\mathbf{r}\ [\chi\phi_A\phi_B - w_A\phi_A - w_B\phi_B - \eta(1 - \phi_A - \phi_B)] - n \ln Q[w_A, w_B]$$

and the single chain partition function is

$$Q[w_A, w_B] = \int \mathcal{D}\mathbf{R}_\alpha(s)\ \exp\left(-\int_0^1 (\beta U_0 + w(\mathbf{R}_\alpha(s), s))ds\right)$$

Fredrickson, G. H. *The Equilibrium Theory of Inhomogeneous Polymers* **2006**, Clarendon Press: Oxford.

Fundamentals of SCFT

Propagators and Modified Diffusion Equations

If we define following propagators

$$q(\mathbf{r}, s) = \int \mathcal{D}\mathbf{R}_\alpha(s) \exp\left(-\int_0^s (\beta U_0 + w(\mathbf{R}_\alpha(s), s))ds\right) \delta(\mathbf{R}_\alpha(s) - \mathbf{r})$$

$$q^*(\mathbf{r}, s) = \int \mathcal{D}\mathbf{R}_\alpha(s) \exp\left(-\int_s^1 (\beta U_0 + w(\mathbf{R}_\alpha(s), s))ds\right) \delta(\mathbf{R}_\alpha(s) - \mathbf{r})$$

We can evaluate the single chain partition function simply by

$$Q = \int d\mathbf{r}\, q(r, s) q^*(r, s)$$

Propagators can be obtained by solving modified diffusion equations

$$\frac{\partial q(\mathbf{r}, s)}{\partial s} = \nabla^2 q - w_X(\mathbf{r}) q$$

$$\frac{\partial q^*(\mathbf{r}, s)}{\partial s} = \nabla^2 q^* - w_X(\mathbf{r}) q^*$$

Fredrickson, G. H. *The Equilibrium Theory of Inhomogeneous Polymers* **2006**, Clarendon Press: Oxford.

Fundamentals of SCFT

Self-Consistent Field Equations

Mean field approximation is introduced to evaluate the field-based partition function

$$\frac{\delta H}{\delta \phi_A} = 0$$

$$\frac{\delta H}{\delta \phi_B} = 0$$

Which gives a set of SCFT equations

$$w_A = \chi \phi_B + \eta$$

$$w_B = \chi \phi_A + \eta$$

Fredrickson, G. H. *The Equilibrium Theory of Inhomogeneous Polymers* **2006**, Clarendon Press: Oxford.

Applications of SCFT

- Polymer solutions
- Polymer blends
- Block copolymers
- Polyelectrolytes
- Semiflexible polymers
- Liquid crystalline polymers
- Tethered polymers
- Polydisperse polymers
- Polymers under confinements
- ...

Applications of SCFT

Self-Assembled Structures of Diblock Copolymers

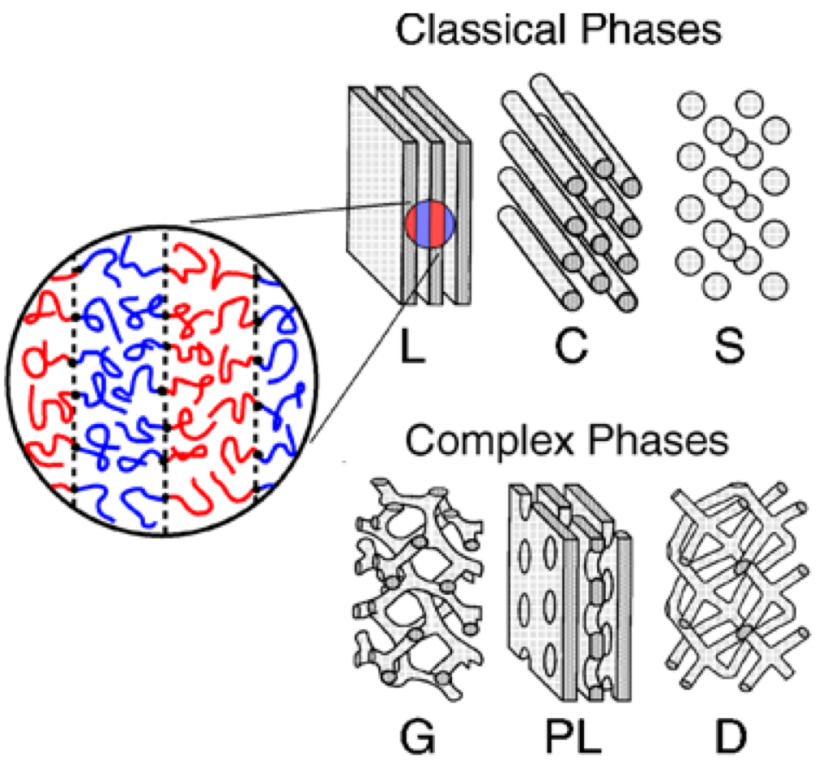

Figure 1. Schematic illustrations of six ordered morphologies showing the domains occupied by the smaller minority blocks. The morphologies can be subdivided into the classical lamellar (L), cylindrical (C) and spherical (S) phases, and the complex gyroid (G), perforated-lamellar (PL) and double-diamond (D) phases. The expanded view of the L phase demonstrates the self-assembly of individual molecules within the morphology.

Matsen, M. W. *J. Phys. Cond. Matter* **2002**, *14*, 21.

Applications of SCFT

Phase Diagram of Diblock Copolymers

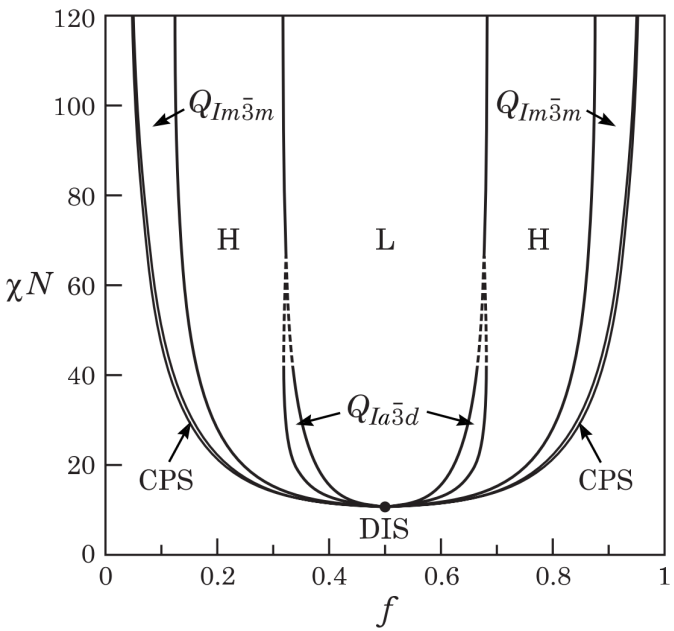

SCFT prediction

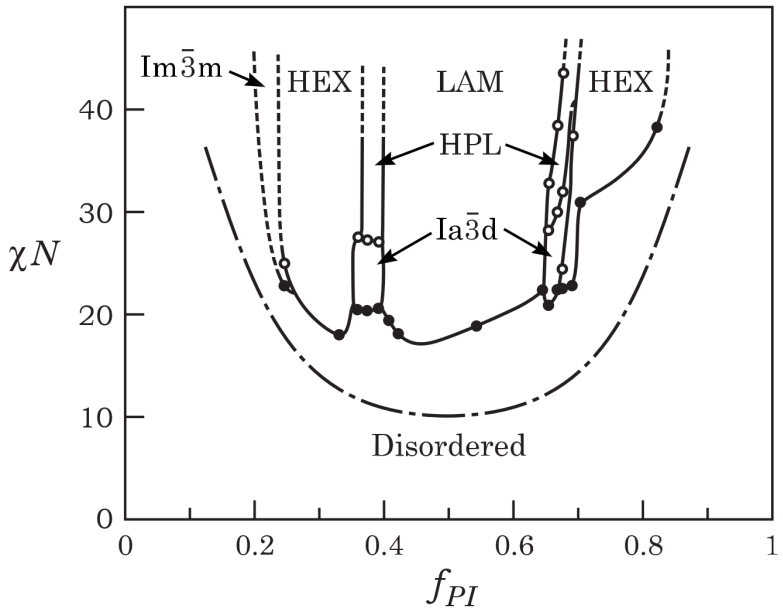

Experimental result

Fredrickson, G. H. *The Equilibrium Theory of Inhomogeneous Polymers* **2006**, Clarendon Press: Oxford.

Applications of SCFT

Diblock-Homopolymer Blends under Cylindrical Confinements

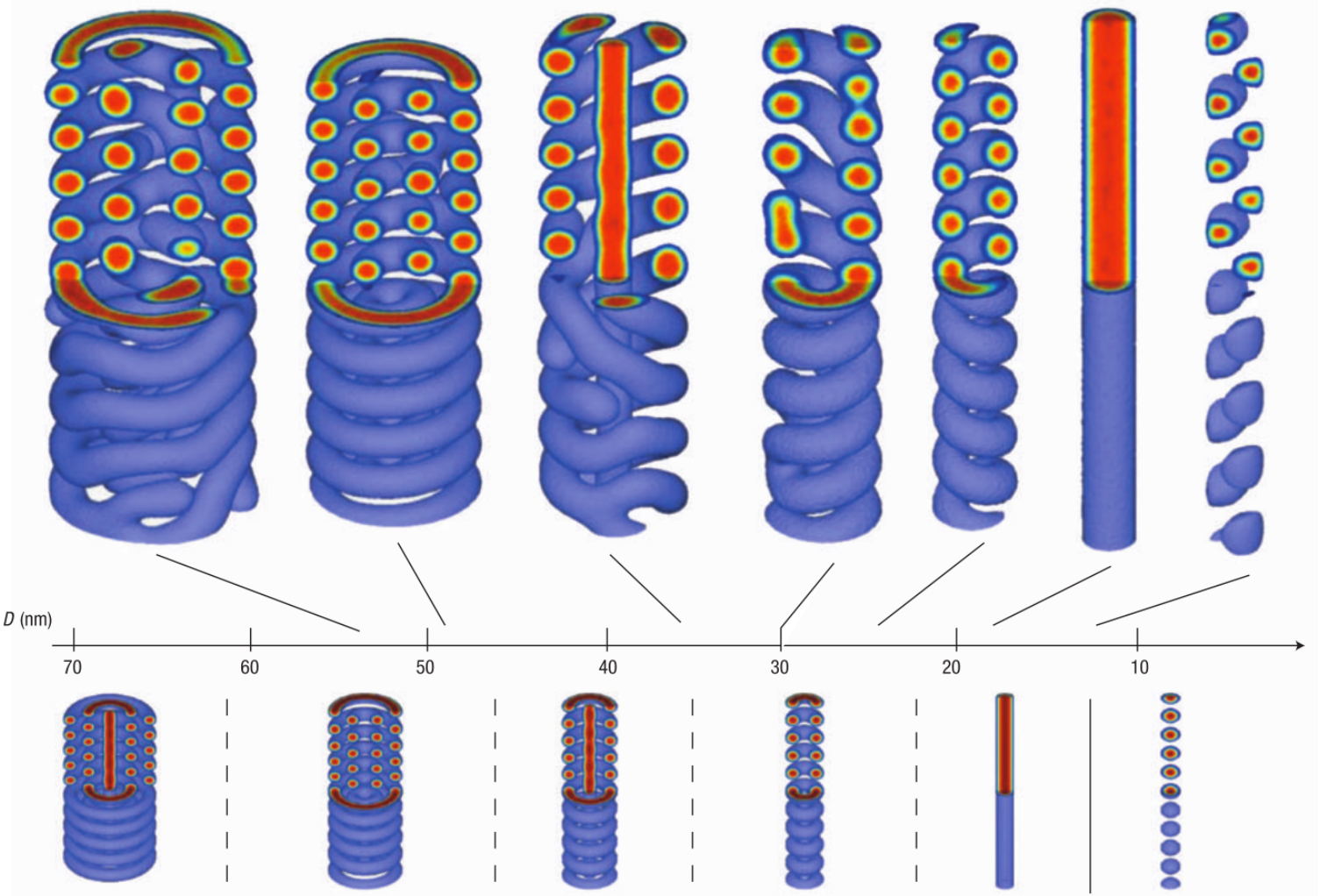

Implementation of SCFT — the `Polyorder` project

- Background
- Design

The Polyorder Project

Background

In most cases, SCFT equations should be solved numerically.

$$w_p = \chi_{ps} N \phi_s(\vec{r}) + \sum_{p \neq p'} \chi_{pp'} N \phi_{p'}(\vec{r}) + \eta(\vec{r})$$

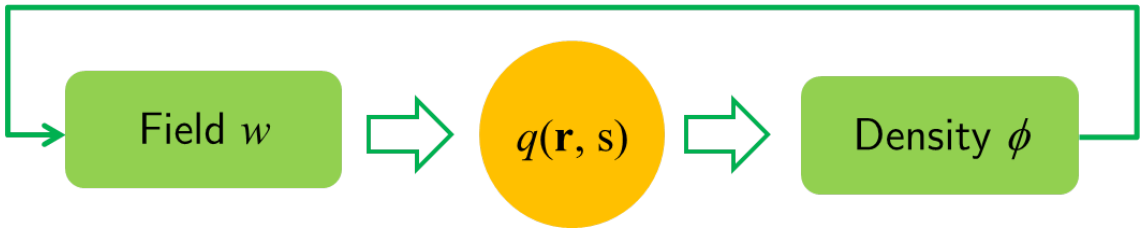

$$\frac{\partial q_p}{\partial s} = \nabla^2 q_p - w_p q_p \qquad \phi_p = \frac{\bar{\phi}_p}{Q_p f_p} \int_0^{f_p} ds q_p(\vec{r}, s) q_p^*(\vec{r}, f_p - s)$$

The Polyorder Project

Overview

The Goal

Polyorder is a C++ library which aims to ease the development of polymer self-consistent field theory (SCFT) programs.

The Framework

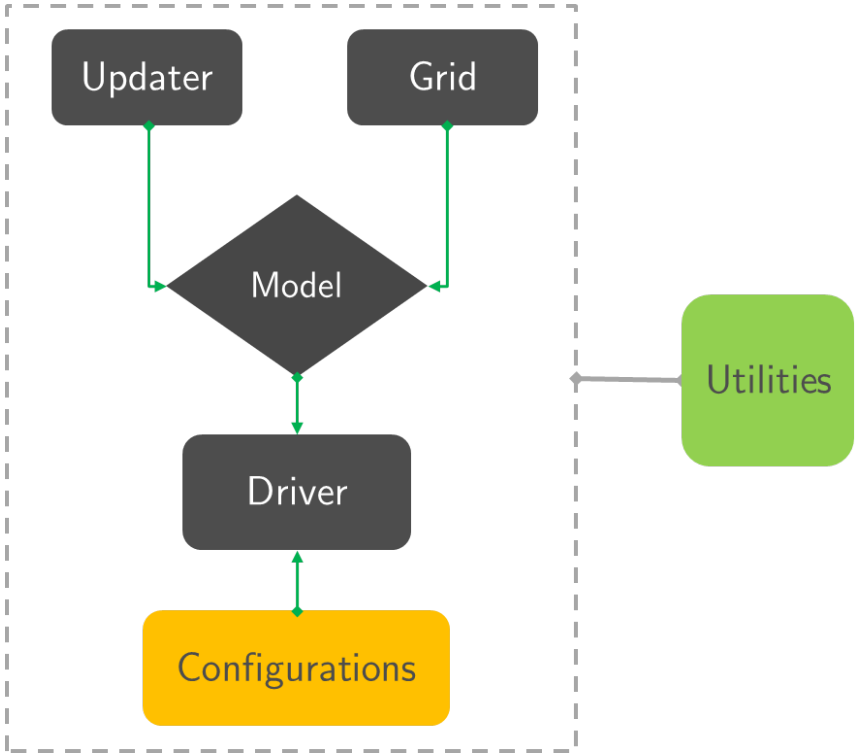

The Polyorder Project

Design

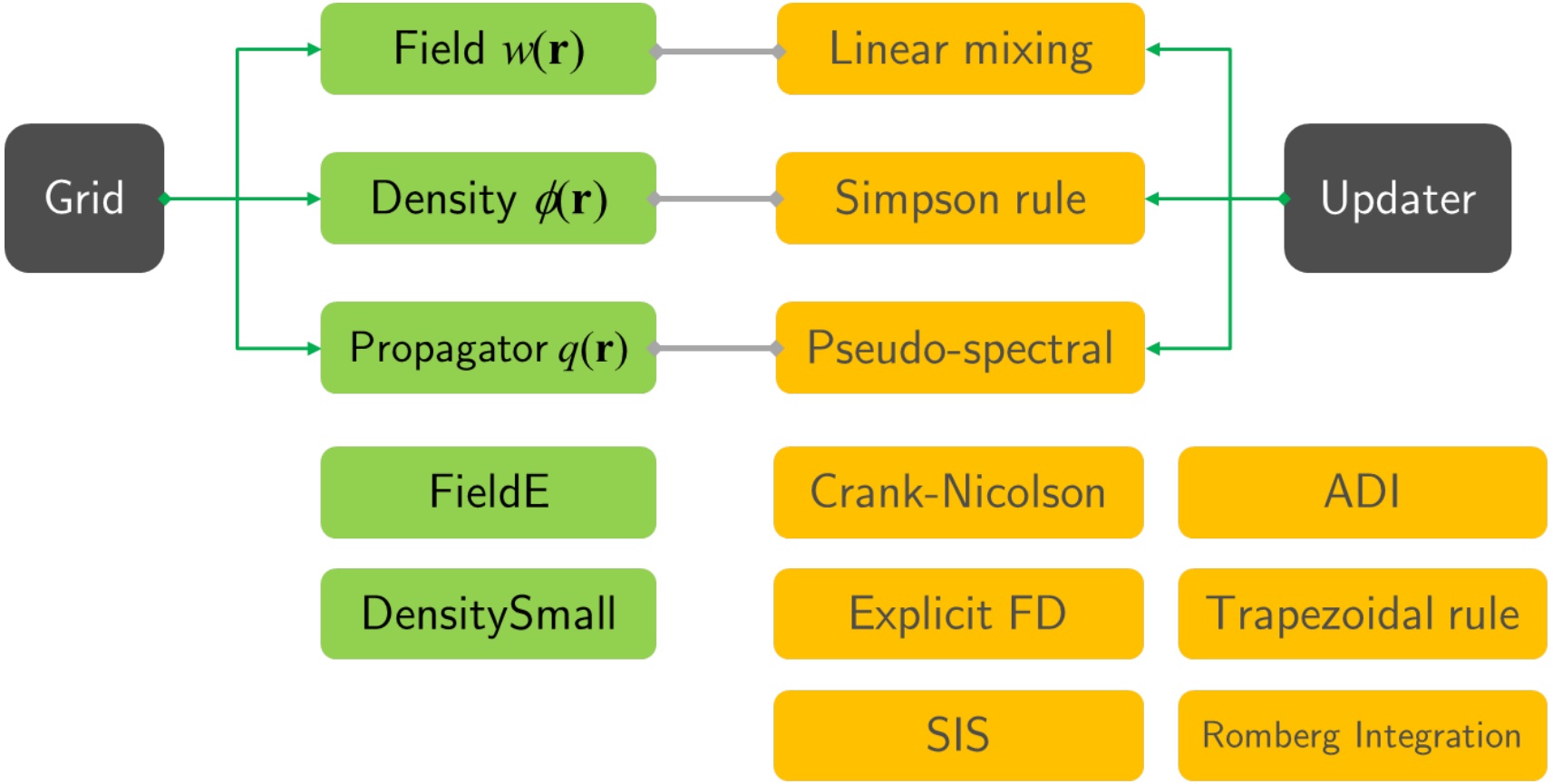

Self-assembly of weakly charged block copolymers

- Introduction
- Numerical Methods
- Results and discussion
- Summary

Introduction

Charged Polymer Solutions and Poisson-Boltzmann Equation

Chain connectivity

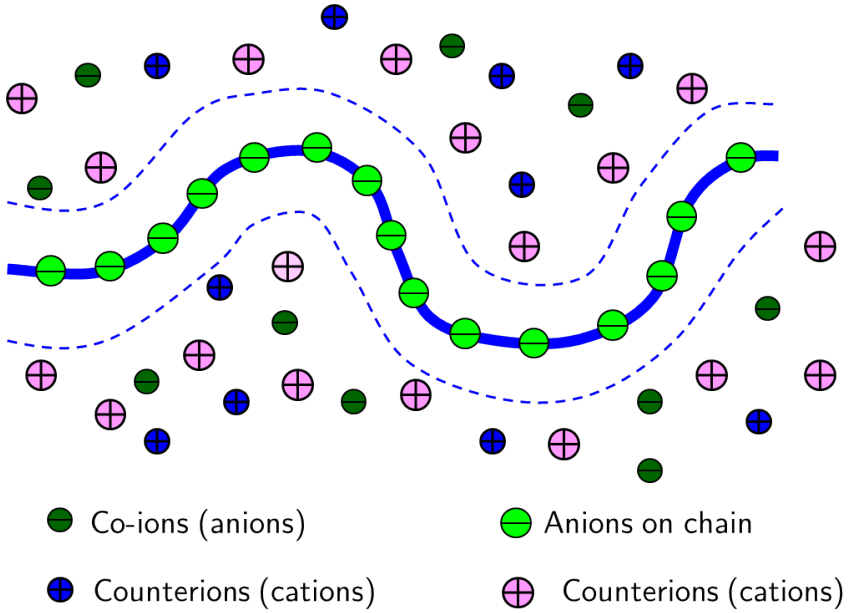

Long range electrostatic interaction

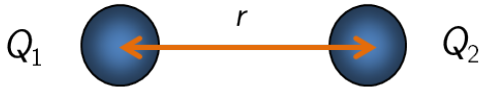

$$U(r) = \frac{Q_1 Q_2 e^2}{4\pi\epsilon\epsilon_0 k_B T} r^{-1}$$

The interaction decays much slower than van der Waals interaction.

In the mean-field level, the electronic interaction can be described by the Poisson-Boltzmann (PB) Equation:

$$\nabla \cdot [\epsilon(\vec{r}) \nabla \psi(\vec{r})] = -N \sum_i \upsilon_i \phi_i(\vec{r})$$

Numerical Methods

The Electric Potential Field

Updated by multigrid Updaters.

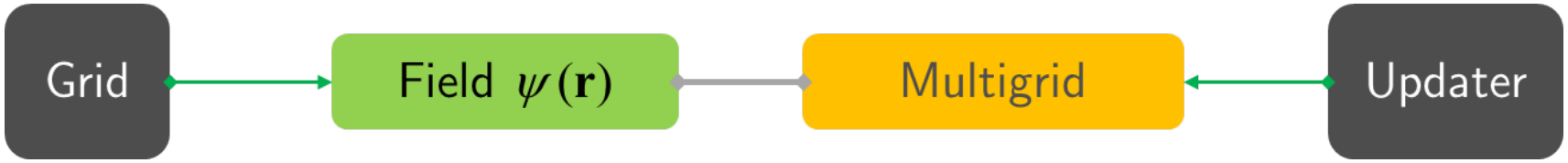

The **Multigrid algorithm** approaches the ideal computational complexity $O(M)$

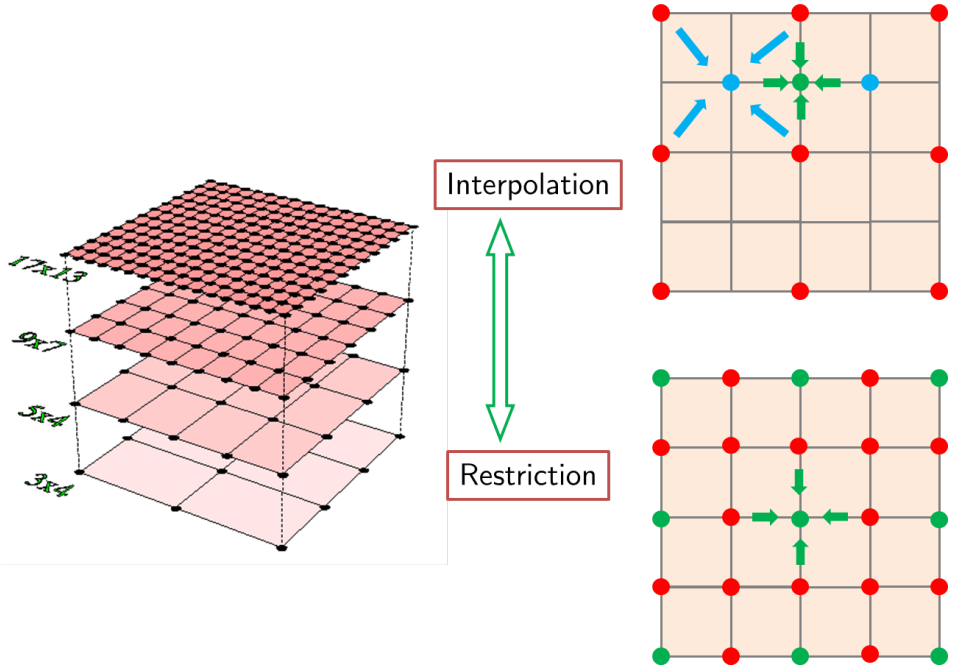

Numerical Methods

Multigrid in Non-orthogonal Unit Cell

For 2D hexagonal unit cell:

$$\nabla \cdot \left[\epsilon\left(\vec{r}\right)\nabla\psi\left(\vec{r}\right)\right] = \frac{4}{3}\epsilon\left(\frac{\partial^2\psi}{\partial x^2} + \frac{\partial^2\psi}{\partial x\partial y} + \frac{\partial^2\psi}{\partial y^2}\right) + \frac{4}{3}\left[\left(\frac{\partial\epsilon}{\partial x} + \frac{1}{2}\frac{\partial\epsilon}{\partial y}\right)\frac{\partial\psi}{\partial x} + \left(\frac{\partial\epsilon}{\partial y} + \frac{1}{2}\frac{\partial\epsilon}{\partial x}\right)\frac{\partial\psi}{\partial y}\right]$$

For 3D hexagonal unit cell:

$$\nabla \cdot \left[\epsilon\left(\vec{r}\right)\nabla\psi\left(\vec{r}\right)\right] = \frac{4}{3}\epsilon\left(\frac{\partial^2\psi}{\partial x^2} + \frac{\partial^2\psi}{\partial x\partial y} + \frac{\partial^2\psi}{\partial y^2} + \frac{3}{4}\frac{\partial^2\psi}{\partial z^2}\right) + \frac{4}{3}\left[\left(\frac{\partial\epsilon}{\partial x} + \frac{1}{2}\frac{\partial\epsilon}{\partial y}\right)\frac{\partial\psi}{\partial x} + \left(\frac{\partial\epsilon}{\partial y} + \frac{1}{2}\frac{\partial\epsilon}{\partial x}\right)\frac{\partial\psi}{\partial y} + \frac{3}{4}\frac{\partial\epsilon}{\partial z}\frac{\partial\epsilon}{\partial z}\right]$$

Results and Discussion

Phase Digram of Charged-Neutral Diblock Copolymer Solutions in 2D Space

Two features of the phase diagram:

1. The critical point moves upward.
2. The diagram is asymmetric.

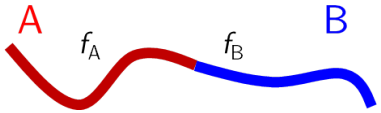

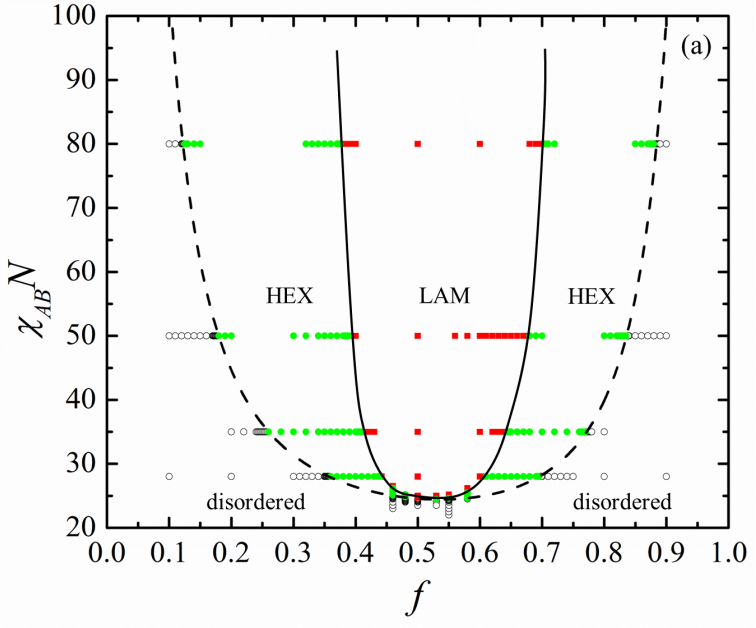

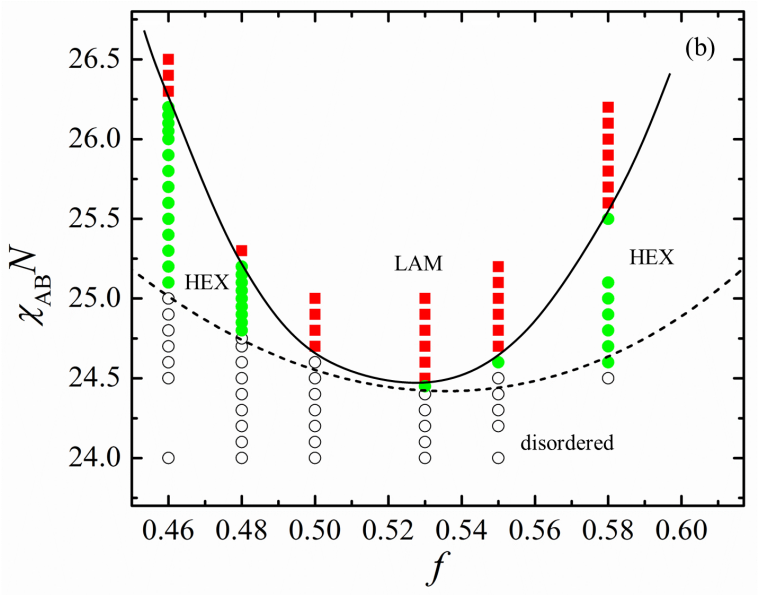

Results and Discussion

Morphologies of Charged-Neutral Diblock Copolymer Solutions in 2D Space

Main predictions:

1. Interfaces of neutral polymers is much sharper than charged polymers.
2. Solvent molecules tends to distribute inside charged domains.

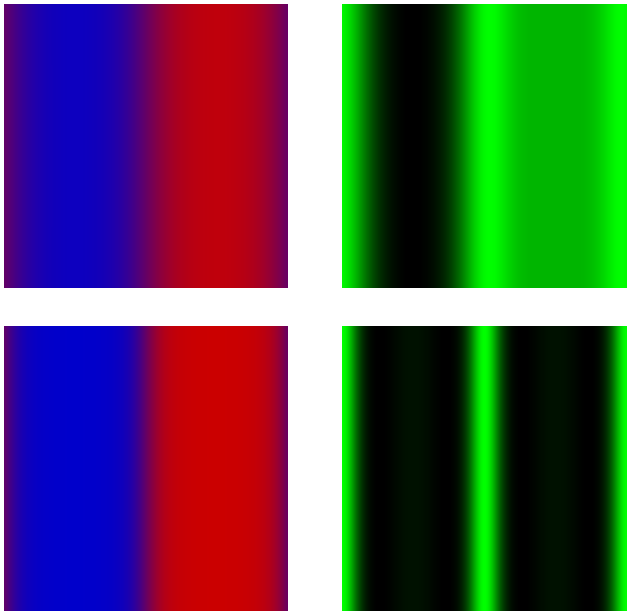

Density distribution of type A (red) and B (blue) segments (left columns), and solvent molecules (right columns) with $f = 0.5$, $\chi_{AB}N = 35$.

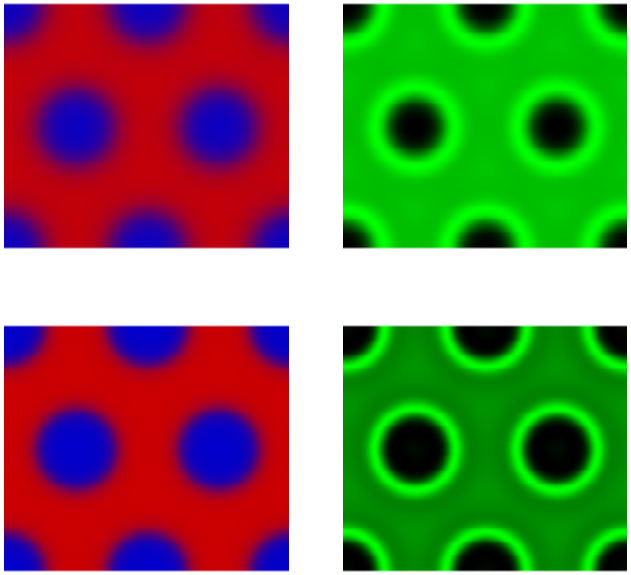

Density distribution of type A (red) and B (blue) segments (left columns), and solvent molecules (right columns) with $f = 0.7$, $\alpha_A N = 20$.

Results and Discussion

Possible Morphologies in 3D

For position-independent dielectric constant

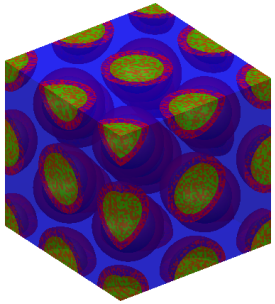

$fA = 0.24$
$\chi_{AB}N = 35$
$\alpha_A N = 2$

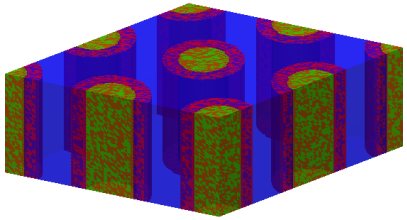

$fA = 0.3$
$\chi_{AB}N = 20$
$\alpha_A N = 2$

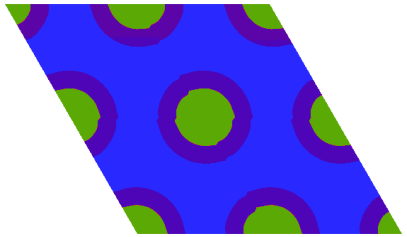

Top view

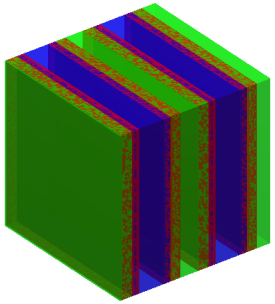

$fA = 0.5$
$\chi_{AB}N = 20$
$\alpha_A N = 2$

For position-dependent dielectric constant

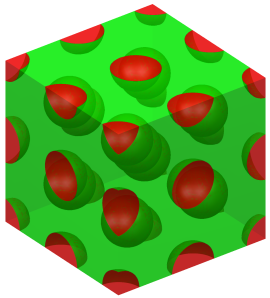

$fA = 0.24$
$\chi_{AB}N = 35$
$\alpha_A N = 2$

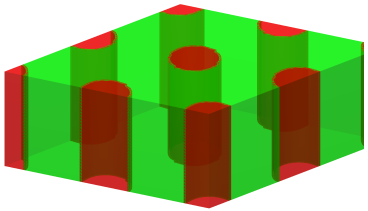

$fA = 0.3$
$\chi_{AB}N = 20$
$\alpha_A N = 2$

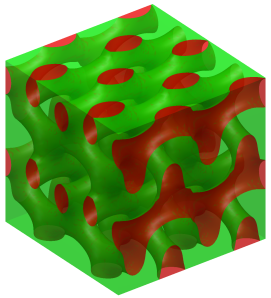

$fA = 0.38$
$\chi_{AB}N = 20$
$\alpha_A N = 2$

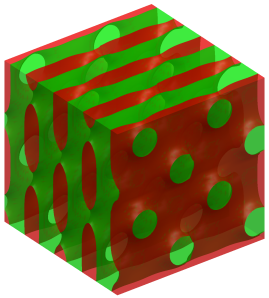

$fA = 0.4$
$\chi_{AB}N = 20$
$\alpha_A N = 2$

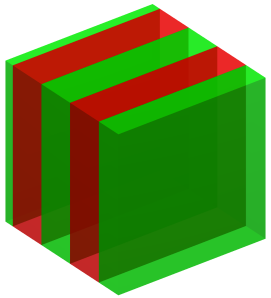

$fA = 0.5$
$\chi_{AB}N = 20$
$\alpha_A N = 2$

Self-assembly of block copolymers confined by interacting walls

- Introduction
- Numerical Methods
- Performance of ETDRK4 Methods
- Applications of ETDRK4 Methods
- Summary

Introduction

Self-Assembly of Block Copolymers under Confinements

In practice, most of block copolymers are more or less under confinement.

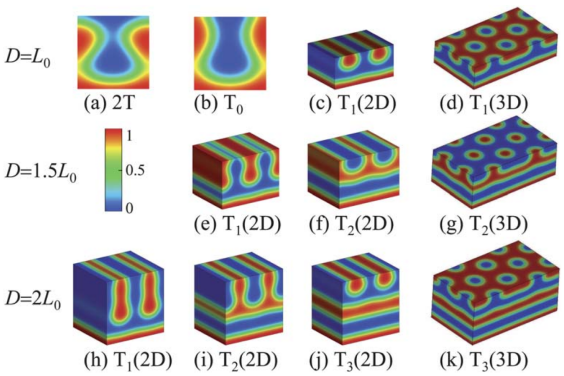

Self-assembly in thin films

D. Meng et al. *Soft Matter* **2010**, *6*, 5891

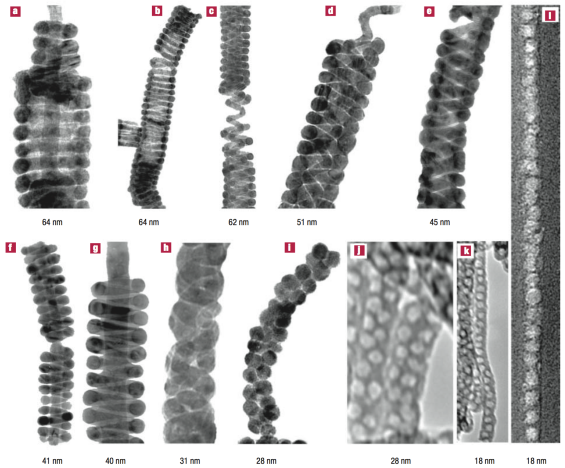

Self-assembly in nanopores

Y. Wu et al. *Nat. Mater.* **2004**, *3*, 816

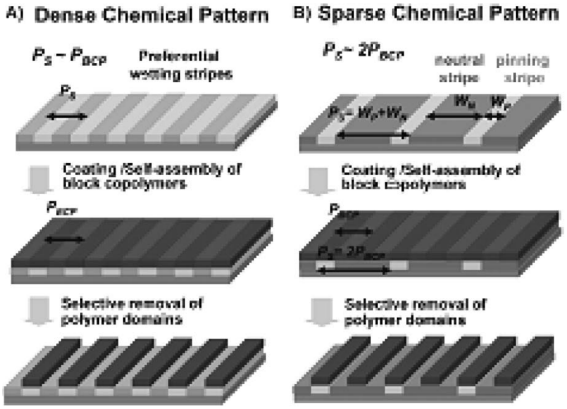

Directed self-assembly (DSA)

H. Kim et al. *Chem. Rev.* **2010**, *110*, 146

Surface and interfacial effects play an important role in determining the self-assemble structures.

Introduction

Modeling Surface and Interfacial Effects in Self-Consistent Field Theory (SCFT)

Approach I:
Using a masking technique and introducing surface interaction terms.

Approach II:
Imposing Robin boundary conditions on the modified diffusion equations for propagators.

$$\frac{\partial q}{\partial n} + \kappa q = 0 \quad \text{at the boundary}$$

Introduction

SCFT Methods for Confined Block Copolymers

Operator splitting with Fourier collocation (OSF, OSS, OSC).

- Fast, $O(M \log M)$.
- Often 2nd order convergence in temporal domain.
- Accuracy degradation for Dirichlet and Neumann boundary conditions (DBC and NBC).
- Not applicable for Robin boundary conditions (RBC).

Operator splitting with Cheyshev collocation (OSCHEB).

- $O(M \log M + \alpha M)$ with large coefficients α.
- Often 2nd order convergence in temporal domain.
- Can handle RBC but requires even larger coefficients.

Other real space methods (finite difference), spectral methods.

Numerical Methods

Exponential Time Differencing Scheme

Modified diffusion equation in matrix form

$$\frac{\partial q}{\partial s} = \mathbf{L}q + \mathbf{F}(q, s)$$

In exponential form

$$\frac{\partial}{\partial s} e^{-\mathbf{L}s} q = e^{-\mathbf{L}s} \mathbf{F}(q, s)$$

Stepping a single contour step

$$q(s_{n+1}) = e^{\mathbf{L}s} q(s_n) + e^{\mathbf{L}s} \int_0^h d\tau \mathbf{F}\left[q(s_n + \tau), s_n + \tau\right]$$

Then a 4th order Runge-Kutta method is employed to approximate the integral.

Numerical Methods

Chebyshev Collocation and Boundary Conditions

To efficiently handle non-periodic boundary conditions, we discretize spatial variables on a Chebyshev-Gauss-Lobatto grid with a set of points

$$x_j = \cos\left(\frac{\pi j}{N}\right), \quad j = 0, 1, \ldots, N$$

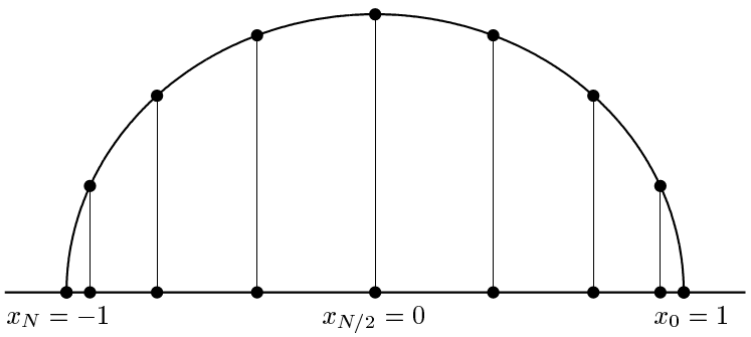

- **L** can be constructed from the Chebyshev differentiation matrix **D**.
- Boundary conditions are imposed by incorporating appropriate terms in **L**.

Performance of ETDRK4

Convergence in Temporal Domain

ETDRK4 exhibits 4th order accuracy in temporal domain.

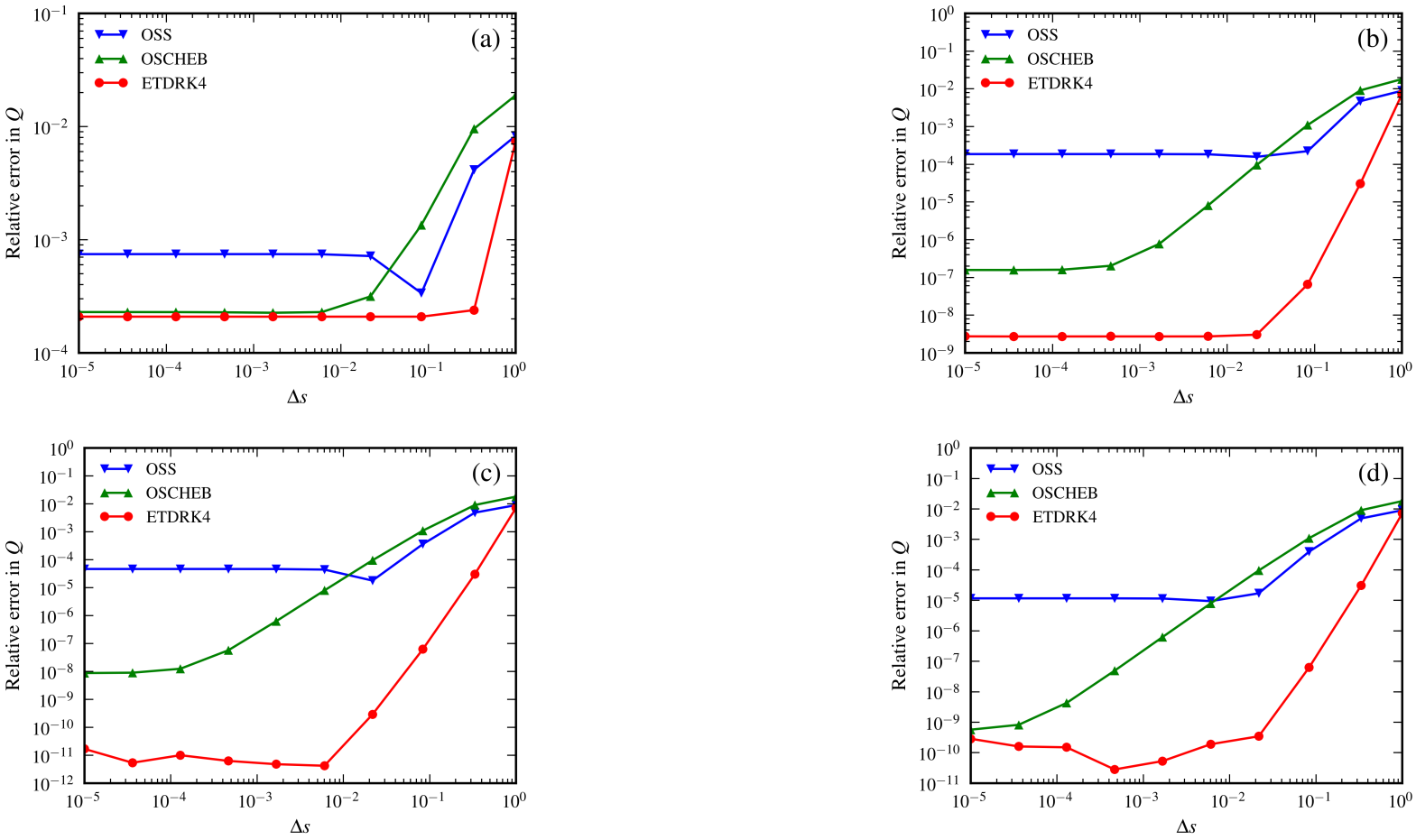

(a) $N = 32$, (b) $N = 64$, (c) $N = 128$, (d) $N = 256$

Performance of ETDRK4

Convergence in Spatial Domain

ETDRK4 retains spectral convergence in spatial domain.

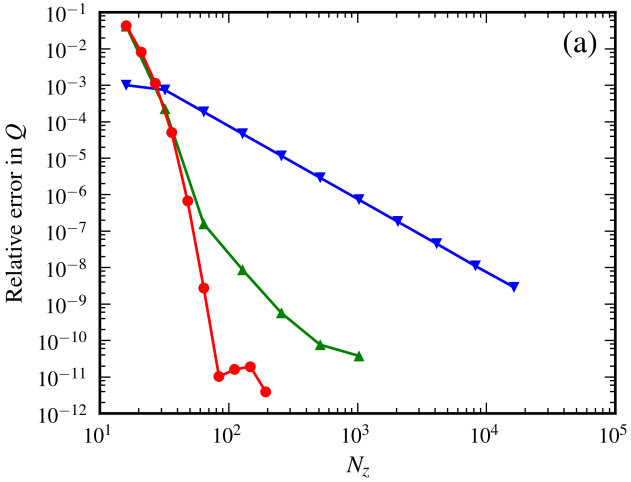

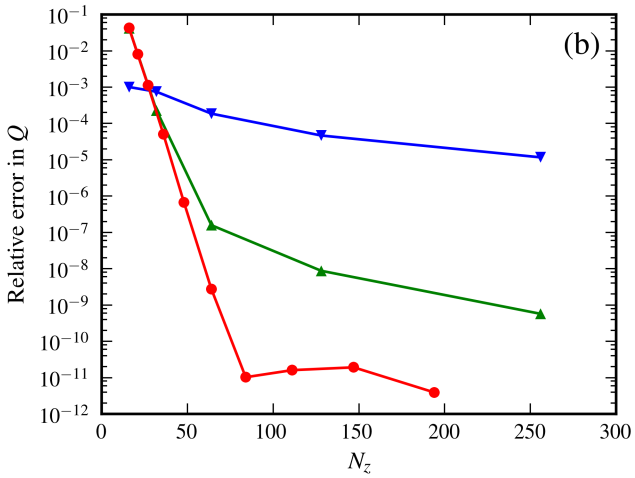

(a) log-log plot, (b) semilog plot. Disk: ETDRK4, up triangle: OSCHEB, down triangle: OSS.

Performance of ETDRK4

Computational Cost

For high accuracy calculations (error$< 10^{-6}$), ETDRK4 is more efficient than OSS and OSCHEB.

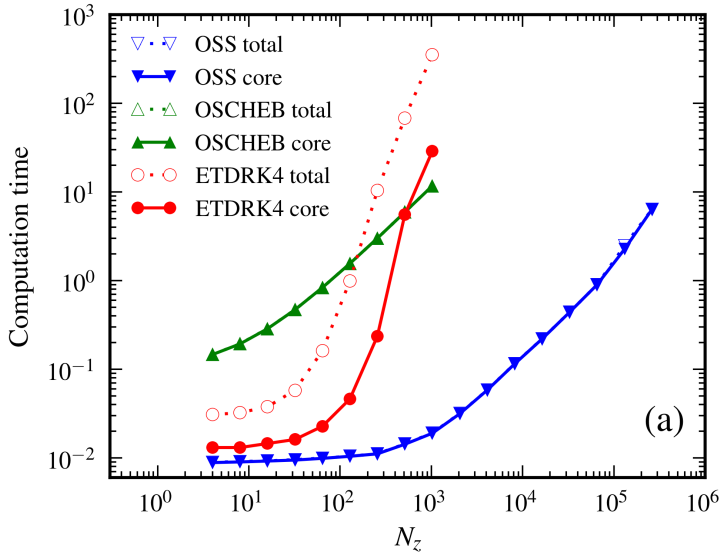

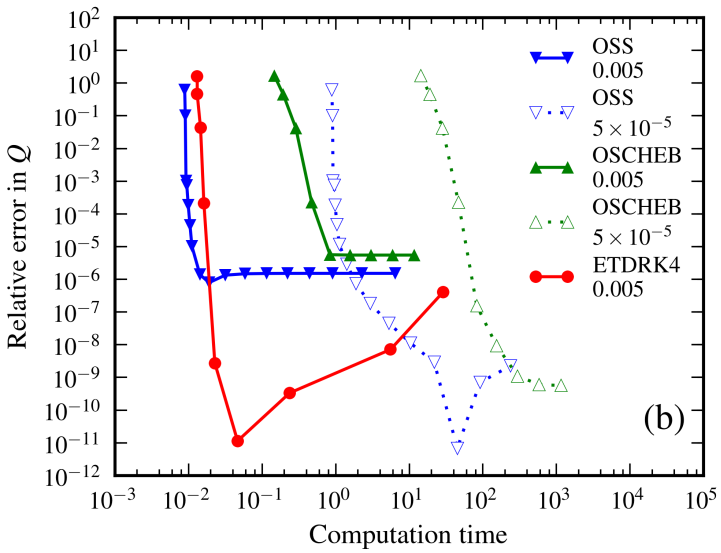

Performance of ETDRK4

Full SCFT Calculations

With ETDRK4, the SCFT algorithm also converge exponentially.

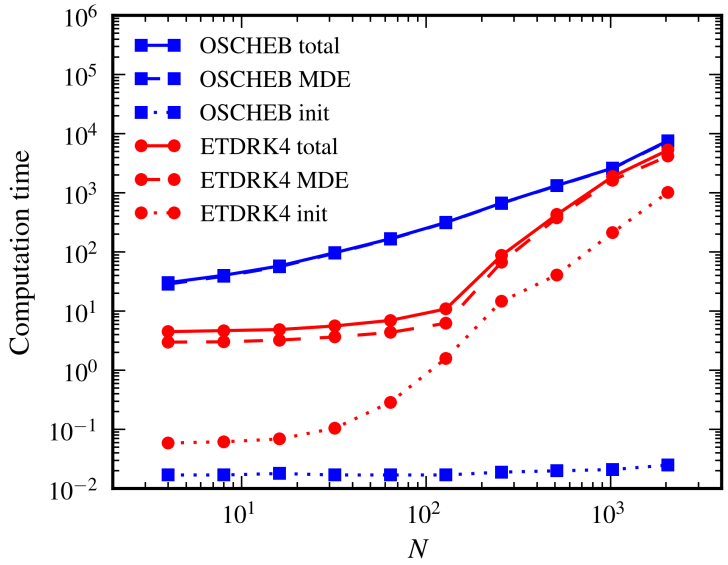

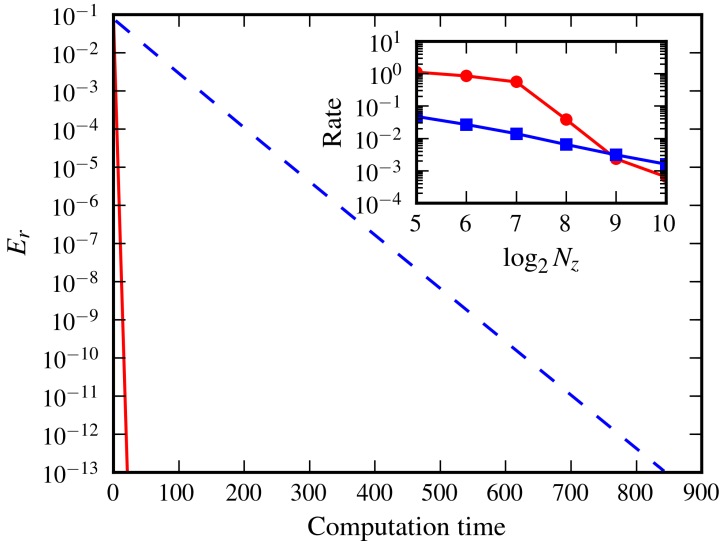

Applications of ETDRK4

Free Energy Calculations

AB diblock copolymer confined by two parallel flat surfaces.

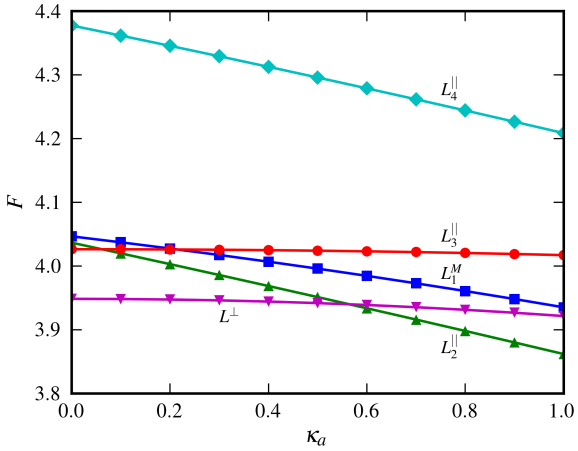

Symmetric surface interactions

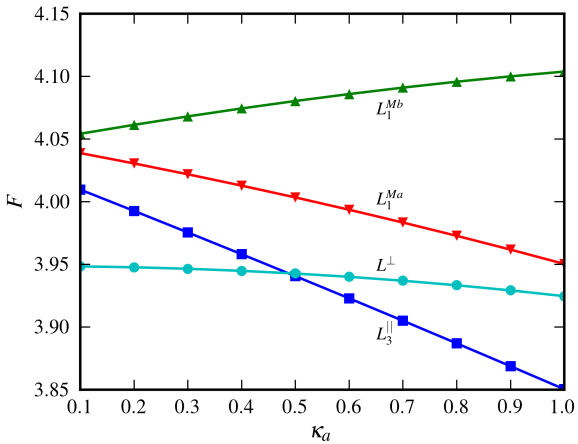

Asymmetric surface interactions

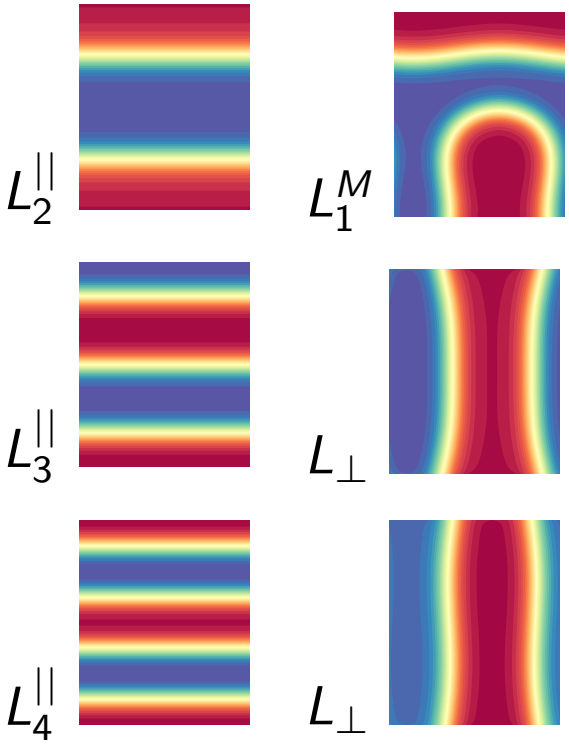

Applications of ETDRK4

3D calculations

AB diblock copolymers confined by two parallel flat surfaces.

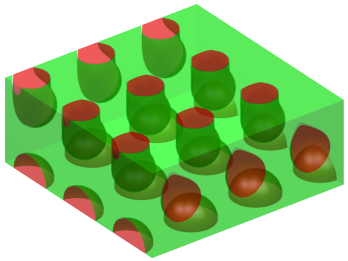

$\kappa_a = 0$

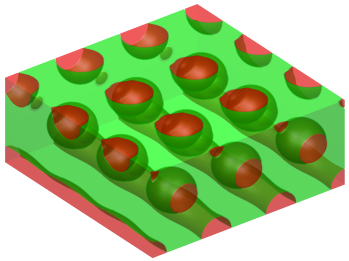

$\kappa_a = 1$

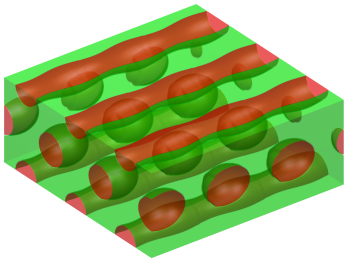

$\kappa_a = 2$

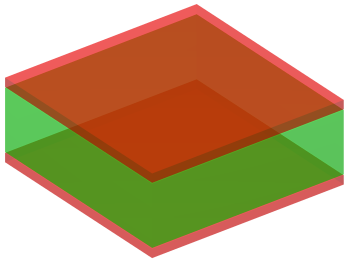

$\kappa_a = 3$

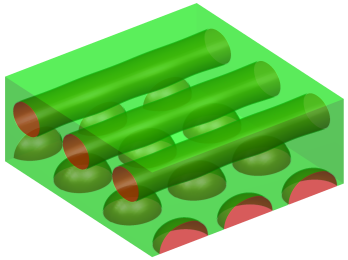

$\kappa_a = -0.1$

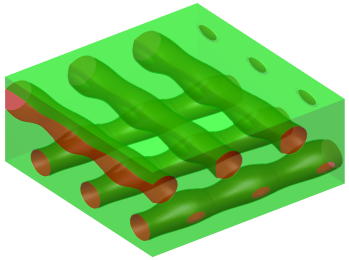

$\kappa_a = -0.2$

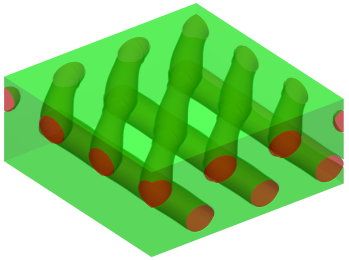

$\kappa_a = -0.3$

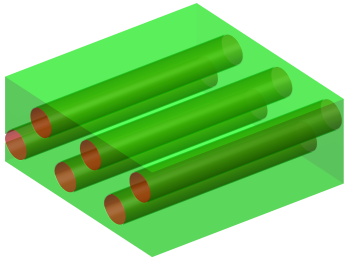

$\kappa_a = -0.5$

Summary

ETDRK4 methods

- Fast for high accuracy calculations.
- 4th order accuracy in temporal domain.
- Spectral accuracy in spatial domain.
- Applicable to RBC without significant increase of computational cost.

Limitations

- Computational cost increases rapidly for non-periodic boundary conditions in two or more dimensions.

Thermodynamics of polymer brushes on interacting substrates

- Introduction
- Results and Discussion

Introduction

Tethered Polymers and Polymer Brushes

The states of tethered polymers

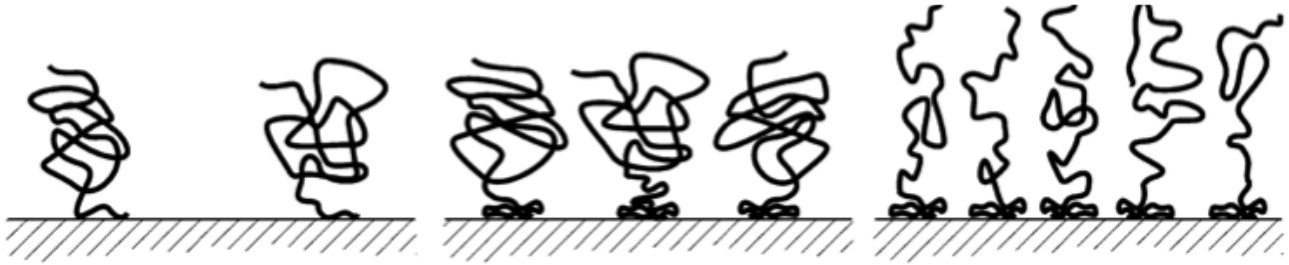

Fig. 21. States of tethered chains: mushroom, overlapping mushroom, brush.

Parabolic density profile for polymer brush

$$\phi(\hat{z}) = \left(\frac{3\pi}{4}\right)^2 - \left(\frac{\pi\hat{z}}{2}\right)^2$$

$$\hat{z} = 2\sqrt{\beta}R_g$$

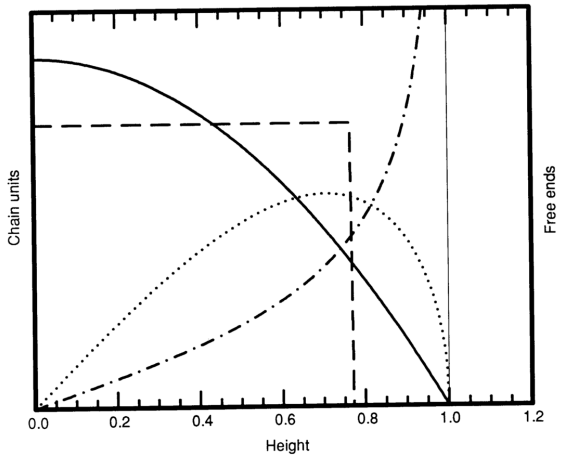

Fig. 2. Chain-unit density profiles $\phi(z)$ for a "parabolic" brush (that is, $\phi << 1$ so $\mu \propto \phi$), and the step-function ansatz at equal coverage σ and chain length N. Also shown are end-density profiles for brushes with (dotted) and without (dot-dashed) solvent.

S. Milner *Science* **1991**, *251*, 905

Results and Discussion

Completely Repulsive Surface

There is only one parameter for homopolymer brush

$$\beta = \left(\frac{u_0 \sigma C}{2}\right)^{\frac{2}{3}}$$

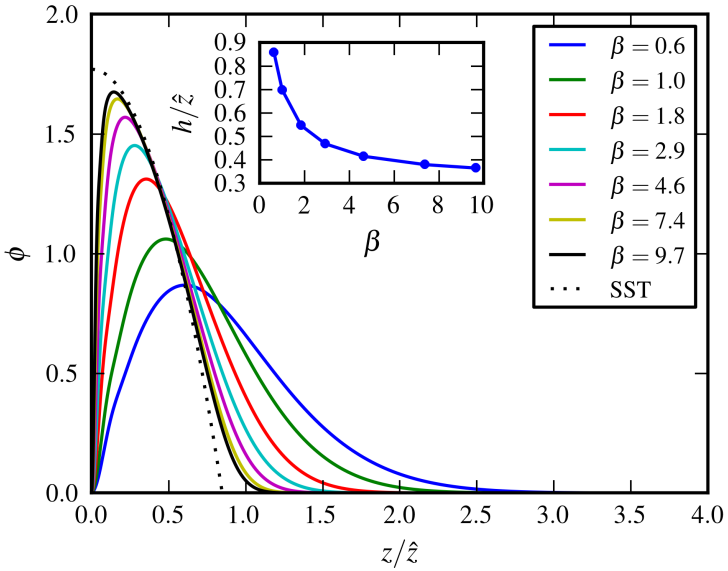

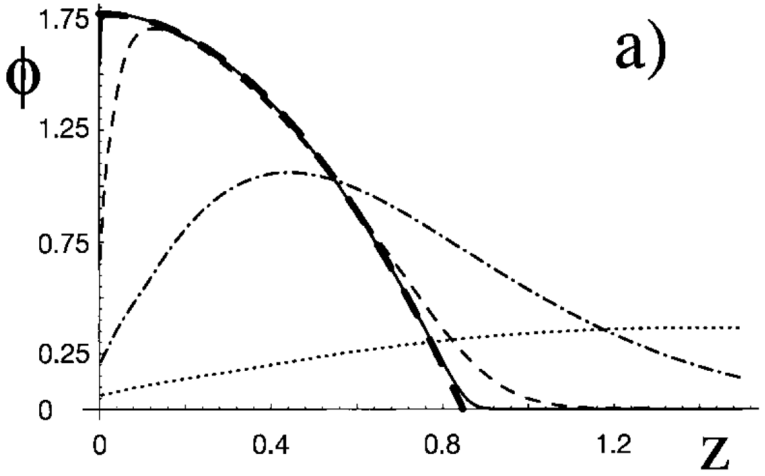

Netz, R. R.; Schick, M. *Macromolecules* **1998**, *31*, 5105

Results and Discussion

Profiles for Different Surface Interactions

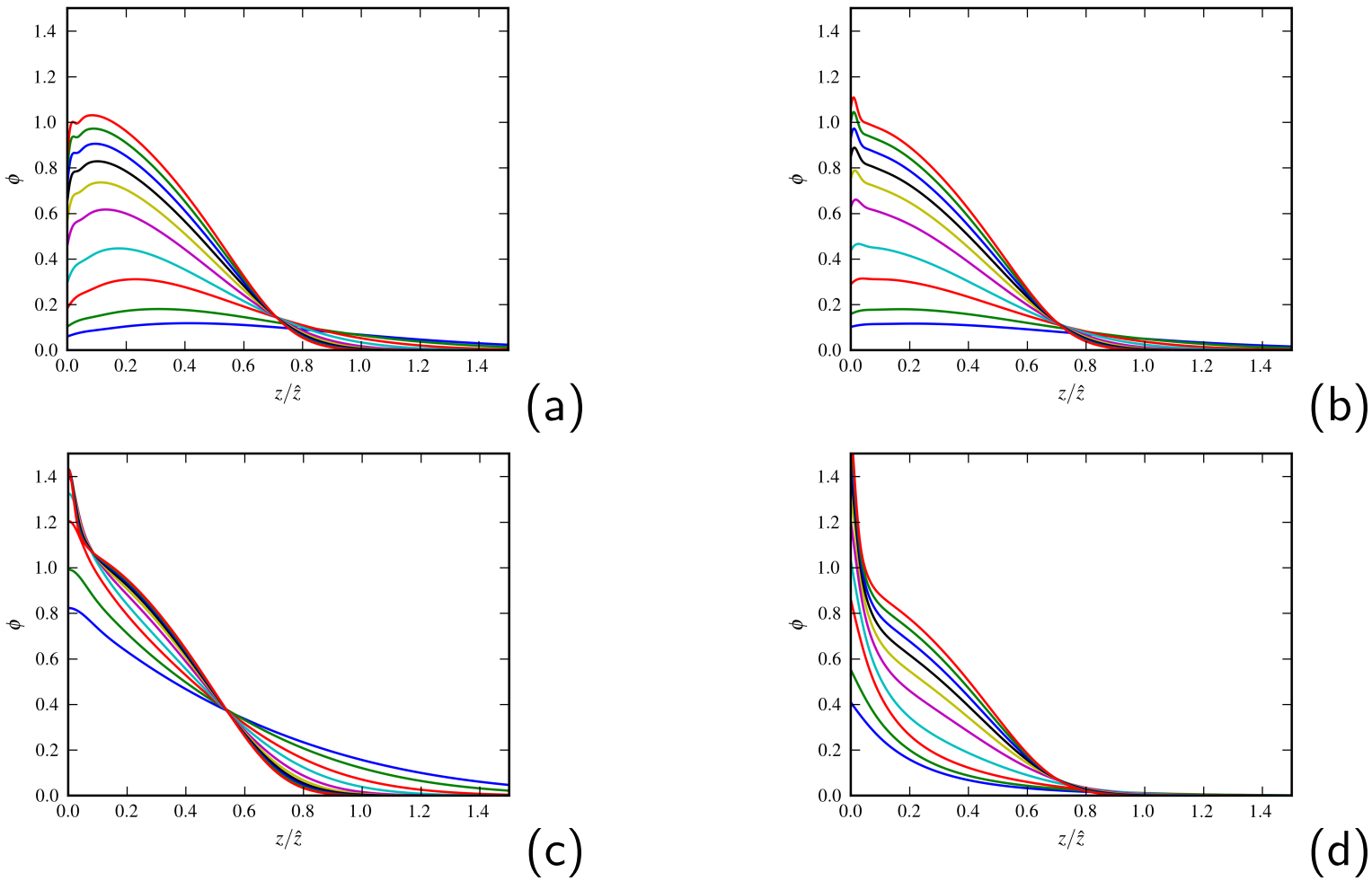

Rescaled segment density profiles as a function of the rescaled distance from the grafting surface calculated by SCFT with (a) $\kappa_a = -10$, (b) $\kappa_a = -4$, (c) $\kappa_a = 0$, and (d) $\kappa_a = 5$. For each part, the values of β for profiles from bottom to top are 0.6, 1.0, 1.8, 2.9, 4.6, 6.1, 7.4, 8.5, 9.7, and 10.7, respectively.

Results and Discussion

Scaling Regions of Tethered Polymers

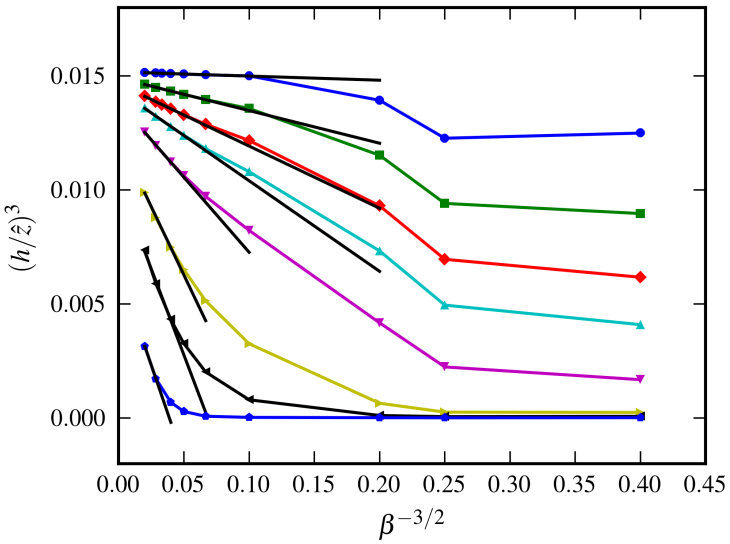

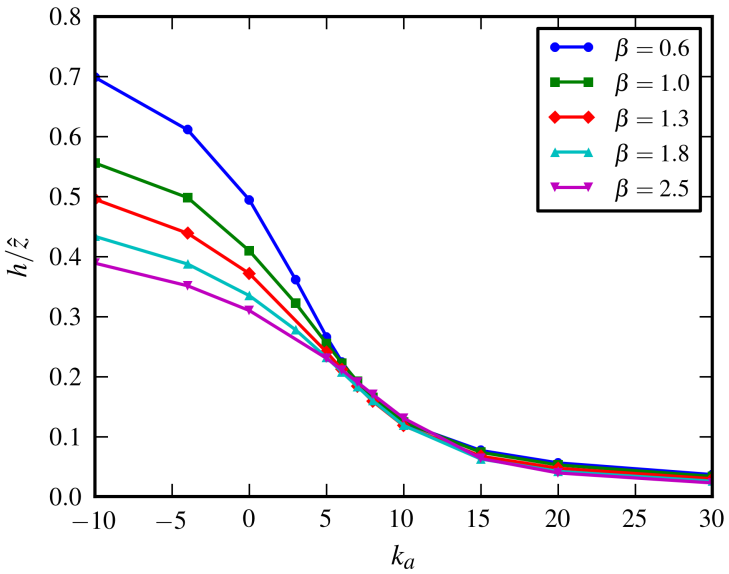

Left: The rescaled brush heights as a function of β for different κ_a. The curves from top to bottom correspond to $\kappa_a = 5, 6, 7, 8, 10, 15, 20$, and 30, respectively.

Right: The rescaled brush heights as a function of κ_a some small βs which are listed in the legend.

Results and Discussion

Phase Diagram of Tethered Polymers

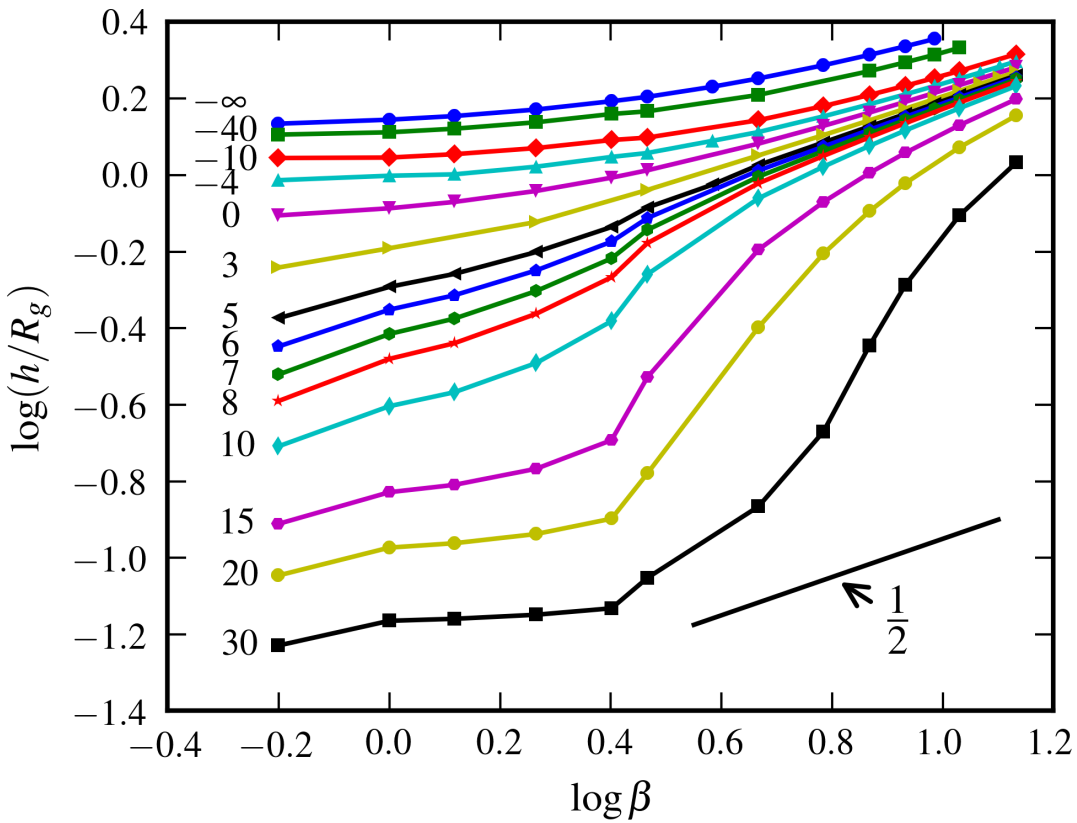

The logarithm of brush heights in unit of R_g as a function of the logarithm of the parameter β for different surface affinities of the grafting surface. The numbers listed in the left of profiles are the value of κ_a. The straight line at the right bottom corner indicate the power law $h/R_g \sim \beta^{1/2}$.

Summary

- We developed highly efficient SCFT methods.
  - A software framework — `Polyorder`
  - Multigrid method for charged polymers.
  - ETDRK4 method for confined polymers and polymer brushes.
- On study of weakly charged polymers.
  - Phase diagram is constructed based on the 2D SCFT calculations.
  - Self-assembled structures are predicted by 3D SCFT calculations.
- On study of block copolymers confined by interacting surfaces.
  - Free energy is evaluated based on the 2D SCFT calculations.
  - Self-assembled structures are predicted by 3D SCFT calculations.
- On study of polymer brushes.
  - Density profiles are predicted.
  - Phase diagram is constructed by scaling analysis of brush height.

Acknowledgments

- Prof. H. D. Zhang, Prof. A. C. Shi
- Prof. F. Qiu, Prof. C. H. Tong, Dr. J. F. Li
- Shanghai Postdoctoral Scientific Program (2011)
- National Natural Science Foundation of China (Grant 21004013)

Thanks!